



Published in final edited form as:

Neuroimage. 2019 May 01; 191: 610–617. doi:10.1016/j.neuroimage.2019.02.022.

Mapping tissue pH in an experimental model of acute stroke – Determination of graded regional tissue pH changes with non-invasive quantitative amide proton transfer MRI

Enfeng Wang^{1,2,‡}, Yin Wu^{1,3,‡}, Jerry S Cheung¹, Takahiro Igarashi¹, Limin Wu⁴, Xiaoran Zhang², and Phillip Zhe Sun¹

¹Athinoula A. Martinos Center for Biomedical Imaging, Department of Radiology, Massachusetts General Hospital and Harvard Medical School, Charlestown, MA, USA

²Department of Radiology, 3rd Affiliated Hospital, Zhengzhou University, Henan, China

³Paul C. Lauterbur Research Centre for Biomedical Imaging, Shenzhen Institutes of Advanced Technology, Chinese Academy of Sciences, Shenzhen, Guangdong, China

⁴Neuroscience Center and Department of Pediatrics, Massachusetts General Hospital and Harvard Medical School, Charlestown, MA, USA

Abstract

pH-weighted amide proton transfer (APT) MRI is sensitive to tissue pH change during acute ischemia, complementing conventional perfusion and diffusion stroke imaging. However, the currently used pH-weighted magnetization transfer (MT) ratio asymmetry (MTR_{asym}) analysis is of limited pH specificity. To overcome this, MT and relaxation normalized APT (MRAPT) analysis has been developed that homogenizes the background signal, thus providing highly pH conspicuous measurement. Our study aimed to calibrate MRAPT MRI toward absolute tissue pH mapping and determine regional pH changes during acute stroke. Using middle cerebral artery occlusion (MCAO) rats, we performed lactate MR spectroscopy and multi-parametric MRI. MRAPT MRI was calibrated against a region of interest (ROI)-based pH spectroscopy measurement ($R^2=0.70$, $P<0.001$), showing noticeably higher correlation coefficient than the simplistic MTR_{asym} index. Capitalizing on this, we mapped brain tissue pH and semi-automatically segmented pH lesion, in addition to routine perfusion and diffusion lesions. Tissue pH from regions of the contralateral normal, perfusion/diffusion mismatch and diffusion lesion was found to be 7.03 ± 0.04 , 6.84 ± 0.10 , 6.52 ± 0.19 , respectively. Most importantly, we delineated the heterogeneous perfusion/diffusion lesion mismatch into perfusion/pH and pH/diffusion lesion mismatches, with their pH being 7.01 ± 0.04 and 6.71 ± 0.12 , respectively ($P<0.05$). To summarize, our study calibrated pH-sensitive MRAPT MRI toward absolute tissue pH mapping, semi-

Corresponding Author: Current Address, Phillip Zhe Sun, Ph.D. (pzhesun@emory.edu), Yerkes Imaging Center, Yerkes National Primate Research Center, Emory University, Department of Radiology and Imaging Sciences, Emory University School of Medicine, 954 Gatewood Road NE, Atlanta, Georgia 30329, Phone: (404) 727-7786.

[‡]These authors contributed equally to this work.

Publisher's Disclaimer: This is a PDF file of an unedited manuscript that has been accepted for publication. As a service to our customers we are providing this early version of the manuscript. The manuscript will undergo copyediting, typesetting, and review of the resulting proof before it is published in its final citable form. Please note that during the production process errors may be discovered which could affect the content, and all legal disclaimers that apply to the journal pertain.

automatically segmented and determined graded tissue pH changes in ischemic tissue and demonstrated its feasibility for refined demarcation of heterogeneous metabolic disruption following acute stroke.

Introduction

pH change is associated with the altered cerebral metabolic rate of oxygen and glucose during the acute stroke (Astrup et al., 1981; Hossmann, 1994; Mehrabian et al., 2018; Siesjo, 1992). In a classic set of studies in the early 1990s, investigators at the Mayo Clinic used optical imaging and showed that pH changes had greater power to define penumbral tissue than blood flow measurements (Anderson et al., 1999; Regli et al., 1995; Tomlinson et al., 1993). However, there has been a lack of non-invasive absolute tissue pH imaging techniques that are suitable for stroke imaging. Although fluorescence imaging has a high spatiotemporal resolution, it is invasive with a limited field of view. Phosphorus MR spectroscopy (MRS), albeit non-invasive, has limited spatiotemporal resolution for acute stroke imaging (Naruse et al., 1983; Smith et al., 1990). To address this, variant chemical exchange saturation transfer (CEST) MRI techniques have been developed recently, including amide proton transfer (APT) and spin-locking MRI (Jin and Kim, 2014; Sun et al., 2007c; Ward et al., 2000; Zhou et al., 2003; Zu et al., 2018). Specifically, APT imaging captures pH-dependent amide proton exchange and has been shown to be sensitive to tissue pH change, complementing perfusion and diffusion MRI (Jokivarsi et al., 2007; McVicar et al., 2014; Sun et al., 2011b; Sun et al., 2012; Sun et al., 2007c; Zhou and van Zijl, 2011). Although magnetization transfer ratio (MTR) is very informative, APT MRI is often quantified by MTR asymmetry (MTR_{asym}) to correct the direct radio frequency (RF) saturation. However, this also makes MTR_{asym} susceptible to concomitant asymmetric MT and nuclear overhauser enhancement (NOE) effects (Heo et al., 2017; Mehrabian et al., 2018; Snoussi et al., 2015; Xu et al., 2016). The currently used pH-weighted APT MRI is of limited pH conspicuity and tissue segmentation is challenging, particularly in the acute stroke setting (Harston et al., 2015).

It has been shown that careful selection of RF saturation field may improve MTR_{asym} conspicuity to cancerous tissue (e.g., APT MRI using a B_1 of about $2\mu\text{T}$ at 3 Tesla MRI). (Zhao et al., 2011) Although such an approach works well for tumor APT MRI, we have shown that pH-weighted MTR_{asym} contrast between the ischemic and normal tissue peaks at $0.75\mu\text{T}$ at 4.7T (Sun et al., 2007b). Under such experimental conditions, the commonly used MTR_{asym} , despite being at its peak pH sensitivity, shows notable heterogeneity even in intact tissue. Because the intact brain white matter and gray matter (WM and GM) have little pH difference (Zhu et al., 2012), the pH-sensitive APT effect shall be relatively uniform. Therefore, the MTR_{asym} inhomogeneity can be largely attributed to concomitant RF irradiation effects such as MT variation across the brain. This suggests that although MTR_{asym} is pH sensitive, its conspicuity needs to be improved. When a weak RF saturation pulse is used, it has been shown that MTR_{asym} is dominated by pH-dependent amide proton exchange in focal ischemia and the apparent NOE (-3.5 ppm) signal is not strongly pH-dependent (Jin et al., 2013; Wu et al., 2018; Zhang et al., 2016) and global ischemia models (Zhou et al., 2019). Recently, it has been demonstrated that magnetization transfer and

relaxation-normalized APT (MRAPT) analysis considerably minimizes confounding non-pH contributions, revealing mismatches among perfusion, pH-weighted and diffusion lesions (Guo et al., 2016). Although MRAPTR is based on MTR_{asym} , it is of much higher pH conspicuity that allows semi-automatic pH lesion segmentation, which is not feasible if using MTR_{asym} .

Our study aimed to further develop MRAPT imaging toward absolute brain pH mapping, refine ischemic tissue classification and determine regional pH changes. Because tissue lactate is highly correlated with pH determined from 31P MRS during the acute stroke (Chang et al., 1990; Hohn-Berlage et al., 1989; Katsura et al., 1992), we determined pH from lactate spectroscopy and calibrated MRAPT MRI in a rodent model of acute stroke, enabling high resolution pH imaging. We measured pH from the diffusion lesion (core) and perfusion/diffusion lesion mismatch, an imaging approximation of the ischemic penumbra (Warach, 2003). Moreover, we semi-automatically segmented ischemic tissue, and delineated the perfusion/diffusion lesion mismatch into perfusion/pH mismatch and pH/diffusion mismatch that likely represent benign oligemia and metabolic penumbra, respectively (Kidwell et al., 2004; Sun et al., 2007c). Our results demonstrated non-invasive tissue pH imaging that complements routine stroke MRI for refined tissue classification.

Theory

The *in vivo* MTR_{asym} can be generally described by (Zhou et al., 2004)

$$MTR_{\text{asym}} = \frac{f_s \cdot k_{\text{sw}}(\text{pH})}{R_{1w}} + MTR'_{\text{asym}} \quad (1)$$

where R_{1w} is the bulk water longitudinal relaxation rate, MTR'_{asym} is an intrinsic MTR asymmetry shift not related to pH, and f_s and k_{sw} are labile amide proton concentration relative to the water proton concentration and its exchange rate, respectively. During acute stroke, the labile proton concentration shows relatively small change and MTR_{asym} is sensitive to the pH-dependent exchange rate (Zhou et al., 2003). The amide proton exchange rate can be described by $k_{\text{sw}} = k_b \cdot 10^{\text{pH} - \text{pH}_b} + k_a$, where k_a and k_b are acid- and base-catalyzed exchange rate, respectively. For *in vivo* APT MRI, MTR_{asym} can be generally described by

$$MTR_{\text{asym}} \propto C_0 \cdot 10^{C_1 \cdot \text{pH}} + C_2 \quad (2)$$

where C_0 and C_1 are constant coefficients due to pH-dependent amide proton exchange rate and R_{1w} , and C_2 is non-pH related baseline shift, which can be determined from pH calibration. Although R_{1w} may be sensitive to pH change during acute stroke, its magnitude of change is much smaller than that of pH-sensitive APT MRI. Therefore, it is reasonable to treat R_{1w} as pH-independent when we quantify APT MRI (Sun et al., 2007c). Tissue pH can be derived from MTR_{asym} as

$$\text{pH} = \log_{10} \left(\frac{\text{MTR}_{\text{asym}} - C_2}{C_0} \right) / C_1 \quad (3)$$

However, $\text{MTR}'_{\text{asym}}$ is heterogeneous across the brain, and pH measurement using the simplistic MTR_{asym} is difficult.

Because pH difference in the intact cerebral tissue is small (Zhu et al., 2012), MTR_{asym} heterogeneity is dominated by non-pH contrast (Guo et al., 2016; Wu et al., 2012). We have

$$R_{1w} \cdot \text{MTR}_{\text{asym}} = f_s \cdot k_{\text{sw}}(\text{pH}) + R_{1w} \cdot \text{MTR}'_{\text{asym}} \quad (4)$$

The heterogeneity in the intact tissue (i.e., $R_2 \cdot \text{MTR}$) can be generally described by a regression function $F(R_{1w}, \text{MMTR})$ based on the relaxation and MT contrast. The MRAPTR analysis takes the difference between experimentally measured T_{1w} -normalized MTR_{asym} and the baseline estimated from the intact tissue, being

$$\Delta\text{MRAPTR} = R_{1w} \cdot \text{MTR}_{\text{asym}} - F(R_{1w}, \text{MMTR}) \quad (5)$$

where MMTR is the mean MTR at ± 3.5 ppm. With the correction of the baseline heterogeneity, MRAPTR is more conspicuous to pH-induced amide proton exchange rate change and we have

$$\begin{aligned} \Delta\text{MRAPTR} &\propto \left\{ \left(C_0 \cdot 10^{C_1 \cdot \text{pH}} + C_2 \right) - \left(C_0 \cdot 10^{C_1 \cdot \text{pH}_{\text{norm}}} + C_2 \right) \right\} \\ &= C'_0 \cdot \left(10^{C_1 \cdot \Delta\text{pH}} - 1 \right) \end{aligned} \quad (6)$$

in which $C'_0 = C_0 \cdot 10^{C_1 \cdot \text{pH}_{\text{norm}}}$, pH_{norm} is the normal tissue pH and $\text{pH} = \text{pH} - \text{pH}_{\text{norm}}$. Tissue pH can be derived from MRAPTR as

$$\text{pH} = \text{pH}_{\text{norm}} + \log_{10} \left(1 + \frac{\Delta\text{MRAPTR}}{C'_0} \right) / C_1 \quad (7)$$

Methods

Animal Stroke Model

The study has been approved by the local Institutional Animal Care and Use Committee, Massachusetts General Hospital. Thirty-five adult male Wistar rats (Charles River Laboratory, Wilmington, MA) were anesthetized initially with 5% and then maintained under 1.5–2.0% isoflurane/air mixture for the duration of the study. Permanent middle

cerebral artery occlusion (MCAO) was induced in rats with a silicone-coated 4–0 nylon filament, and rats underwent MRI about 1 hour after stroke induction. Rats were divided into two groups. Briefly, 15 acute stroke rats underwent multi-parametric MRI and lactate MRS for pH calibration. Two rats displayed ischemic lesion in the ipsilateral hypothalamus, not the middle cerebral artery (MCA) vascular territory, and they were excluded from data analysis. Another group of 20 acute stroke rats underwent multi-parametric MRI to investigate the ischemic lesion heterogeneity (without lactate MRS).

MRS and MRI

Animals were imaged using a 4.7T small-bore scanner (Bruker Biospec, Billerica, MA). Multi-slice MRI (5 slices, slice thickness/gap=1.8/0.2 mm, the field of view=20×20 mm², image matrix=48×48) was acquired with echo planar imaging (EPI). We collected water-suppressed single voxel point resolved spectroscopy (PRESS), relaxation, diffusion, APT and perfusion MRI. Specifically, lactate MRS was acquired from a cubic region of (3.5 mm)³, positioned in the striatum region that is most susceptible to ischemic insult (repetition time (TR)/echo time (TE) = 2000/144 ms, averages = 512, scan time ~ 17 min). pH-weighted MRI was acquired with fast unevenly segmented RF irradiated APT MRI (Sun et al., 2011a). We used a recovery time of 5000 ms, primary RF saturation duration of 4500 ms, and secondary RF saturation duration of 500 ms for an RF irradiation amplitude of 0.75 μT applied at ±3.5ppm. The unsaturated control scan was averaged 8 times, while the saturated images were averaged 32 times (scan time ~ 4 min). Diffusion MRI was obtained using single-shot diffusion-weighted EPI (b-values = 250/1000 s/mm², TR/TE = 3250/54 ms, 16 averages, scan time = 2 min) (Mori and Vanzijl, 1995). For perfusion MRI, we used the amplitude modulated continuous arterial spin labeling (AM-CASL) MRI (TR/TE = 6,500/15 ms, time of saturation = 3250 ms and 32 averages, B₁ = 4.7 μT, scan time ~ 7 min) (Utting et al., 2005). In addition, T_{1w} MRI was acquired with inversion recovery EPI of seven inversion delays from 250 to 3000 ms (TR/TE = 6500/15 ms, 4 averages, scan time = 3 min), and T₂ EPI was obtained with two separate spin echo EPI images with TE of 30 and 100 ms (TR = 3250 ms, 16 averages; scan time = 2 min).

Data Analysis

Spectroscopy data were processed with Java-based Magnetic Resonance User Interface (jMRUI, <http://www.jmrui.eu>) and images were processed in Matlab (Mathworks, Natick, MA). MRAPT MRI was calibrated against previously published raw data of multiparametric MRI and lactate MRS and then applied to determine tissue pH for MRI-defined ischemic regions of perfusion/pH/diffusion lesion mismatch (Guo et al., 2016; Sun et al., 2011b). T_{1w} map was derived by fitting EPI signal as a function of the inversion time

$$I(i) = I_0 \left[1 - (1 - \eta) e^{-TI_i/T_1} \right]$$
, where η is the inversion efficiency and TI_i is the i^{th} inversion time. T₂ and apparent diffusion coefficient (ADC) maps were obtained as

$$T_2 = \frac{\Delta TE}{\ln(I(TE_1)/I(TE_2))}$$
 and
$$ADC = \frac{\ln(I(b_1)/I(b_2))}{\Delta b}$$
, where TE_{1,2} and b_{1,2} are two TEs (30/100

ms) and diffusion b values (250/1000 s/mm²), respectively, with TE and b being their

differences. Cerebral blood flow (CBF) was calculated as $CBF = \frac{\lambda(I_{ref} - I_{tag})}{2\alpha \cdot I_{ref}} \cdot \frac{e^{-w/T_{1a}}}{T_1}$, where

I_{tag} and I_{ref} are the label and the reference image, respectively, λ is the brain-blood partition coefficient for water, α is the degree of inversion with transient time correction, w is the post-labeling delay, and T_{1a} is the arterial blood longitudinal relaxation time. In addition, MTR was calculated as $MTR(\pm 3.5\text{ppm}) = 1 - I(\pm 3.5\text{ppm})/I_0$, where I_0 is the control image without RF irradiation and $I(\pm 3.5\text{ppm})$ are the label and reference images with RF irradiation applied at $\pm 3.5\text{ppm}$, respectively. The mean MTR (MMTR) was calculated as the average of MTRs at $\pm 3.5\text{ppm}$. pH-weighted MTR_{asym} image was calculated as $MTR_{asym} = [I(-3.5\text{ppm}) - I(+3.5\text{ppm})]/I_0$. In addition, MRAPTR was calculated as the difference (i.e. $MRAPTR = R_{1w} * MTR_{asym} - MRAPTR$) between the measurement and that estimated from regression analysis (Guo et al., 2016). Perfusion, pH, and diffusion ischemic lesions were segmented using a K-means clustering-based algorithm, as shown in our prior study (Lu et al., 2018).

Results

Fig.1 shows diffusion and pH-sensitive MRI images from a representative acute stroke rat. The ipsilateral ischemic lesion displayed substantial ADC decrease (Fig. 1a). Lactate MRS was acquired from an ROI positioned in the striatum (overlaid on the ADC image), coinciding with the ischemic insult. The ipsilateral ischemic ROI was mirrored to the contralateral normal tissue for reference. Fig. 1b shows that although pH-weighted MTR_{asym} image revealed hypointensity in the ischemic region, there was noticeable heterogeneity in the intact brain tissue, predominantly between the white matter and grey matter (WM/GM). Because pH difference in the intact cerebral tissue is very small, such image heterogeneity is not pH related (Zhu et al., 2012). MRAPTR (Fig. 1c) minimized non-pH baseline shift and reduced heterogeneity in the intact tissue while capturing the pH-sensitive signal change in the ischemic region.

We calibrated pH-sensitive MTR_{asym} and MRAPTR indices toward absolute tissue pH (Fig. 2). Briefly, lactate, choline, and creatine peaks were determined using jMRUI, and tissue pH was derived from the lactate concentration according to $pH = -0.0335 * [Lac] + 6.83$ (Jokivarsi et al., 2007; Katsura et al., 1992). MTR_{asym} and MRAPTR were numerically fit with respect to pH using Eq. 3 and Eq. 6, respectively. For MTR_{asym} , we had $pH = \log_{10}((100 * MTR_{asym} - C_2)/C_0)/C_1$, with C_0 , C_1 and C_2 found to be 0.46, 0.19 and -13.9 , respectively ($R^2=0.45$, $P<0.05$). For MRAPTR, we had $pH = 7.05 + \log_{10}(MRAPTR / C'_0 + 1)/C_1$, with C'_0 and C_1 found to be 5.04 and 0.25, respectively ($R^2=0.70$, $P<0.001$). It is helpful to point out that C_1 is less than 1. This is likely because in vivo APT signal originates from a composite of exchangeable amide groups of slightly different base-catalyzed relationships (Zhou et al., 2019). Therefore, it is appropriate to calibrate

MRAPTR vs pH using a generalized base-catalyzed relationship. Note that the correlation between MRAPTR and pH is noticeably higher than that of MTR_{asym} (0.70 vs. 0.45), indicating improved pH specificity. We applied the calibration curve and determined pH from both the contralateral normal and ipsilateral ischemic ROIs. Fig. 3 shows pH maps determined from MTR_{asym} (Fig. 3a) and MRAPTR (Fig. 3b), respectively. Table 1 shows

that pH derived from MRAPT MRI has substantially reduced standard deviation in the contralateral intact tissue, confirming its higher pH specificity than the routine MTR_{asym} analysis.

Fig. 4 shows multi-parametric perfusion, diffusion and pH images from a representative acute stroke rat. There was a significant size difference between perfusion, pH and diffusion lesions (one-way ANOVA). Ischemic lesions were segmented based on K-means clustering approach and overlaid on each MRI indices. There was noticeable mismatch among perfusion (Fig. 4a), diffusion (Fig. 4b) and pH lesions (Fig. 4c). The relatively large perfusion lesion confirmed near complete MCA occlusion. Whereas the diffusion lesion core showed the worst pH drop, the peri-infarct perfusion/diffusion lesion mismatch appears to have a mild pH change. Fig. 4d shows perfusion/pH lesion mismatch (red, benign oligemia), pH/diffusion lesion mismatch (green, metabolic penumbra) and diffusion lesion (black, ischemic core). Across 35 rats, these regions represent $21\pm 12\%$, $34\pm 18\%$ and $44\pm 16\%$ of the hypoperfusion lesion, respectively.

Fig. 5 shows multiparametric MRI indices from the diffusion lesion (black triangle), pH/diffusion lesion mismatch (green square), perfusion/pH lesion mismatch (red circle) and perfusion/diffusion lesion mismatch (pink solid circle). The measurements were summarized in Table 2. Fig. 5a shows that although diffusion lesion has significantly reduced ADC ($0.62\pm 0.03 \mu\text{m}^2/\text{ms}$, $P<0.05$, One-way ANOVA with Bonferroni's Multiple Comparison Test) from all three mismatch regions (i.e., pH/diffusion ($\text{ADC}=0.81\pm 0.04 \mu\text{m}^2/\text{ms}$), perfusion/pH ($\text{ADC}=0.82\pm 0.04 \mu\text{m}^2/\text{ms}$) and perfusion/diffusion ($\text{ADC}=0.81\pm 0.04 \mu\text{m}^2/\text{ms}$)), the mismatch regions have substantially overlapped perfusion and diffusion values. Although all ischemic regions have significantly reduced CBF from the contralateral brain ($\text{CBF}=1.59\pm 0.44 \text{ ml/g}\cdot\text{min}$), Fig. 5b shows that only PWI/pH mismatch has significantly higher perfusion level than that of diffusion lesion (0.95 ± 0.33 vs. $0.69\pm 0.33 \text{ ml/g}\cdot\text{min}$, $P<0.05$). Fig. 5c shows that while ADC cannot differentiate perfusion/diffusion, perfusion/pH and pH/diffusion mismatches, their pH was different, being 6.84 ± 0.10 , 7.01 ± 0.04 and 6.71 ± 0.12 , respectively ($P<0.05$, One-way ANOVA with Bonferroni's Multiple Comparison Test). Fig. 5d shows that regions of diffusion lesion, pH/diffusion lesion mismatch, and perfusion/pH lesion mismatch can be resolved using multi-dimensional perfusion, pH and diffusion indices, augmenting routine perfusion and diffusion-based stroke imaging.

Discussion

Our study calibrated MRAPT image toward absolute pH mapping and determined heterogeneous pH change during acute ischemic stroke. We found that pH MRI resolves graded tissue metabolic injury, consistent with the hypothesis that the perfusion/diffusion mismatch includes not only metabolic penumbra but also benign oligemia that is not at risk to infarction (Kidwell et al., 2004; Sun et al., 2007c).

The MRAPT analysis assumes that the background heterogeneity can be described using relaxation and MT MRI. To confirm this assumption, we evaluated multi-parametric MRI and estimated their impact on pH accuracy. Our study used an inversion recovery sequence

to measure T_{1w} map. Although T_{1w} measurement may be susceptible to pH change, the effect shall be small in the absence of the amplification mechanism used by CEST and spinlock MRI. Notably, ischemic tissue T_{1w} was 1.53 ± 0.03 s to 1.65 ± 0.05 s for the contralateral normal and ischemic ROI, respectively, while MMTR showed very little change (0.29 ± 0.01 vs. 0.29 ± 0.00). T_{1w} change may cause a slight overestimation of the background from the regression analysis (from $-2.2\pm 0.1\%$ to $-1.8\pm 0.1\%$). Note that this difference represents a mere $16\pm 5\%$ of the 'ideal' correction without T_{1w} change, equivalent to a pH underestimation of -0.11 ± 0.04 . It is necessary to note that MRAPTR and pH calibration was based on experimentally obtained MRAPTR and T_{1w} , which partially compensates for small T_{1w} change. Therefore, the magnitude of pH error caused by T_{1w} relaxation change is no more than 0.1 pH unit. In addition, the pH measurement error shall be even less in the penumbral tissue than that of the ischemic core due to its less T_{1w} change. As such, quantitative MRAPT analysis provides reasonably accurate pH measurement during acute stroke with the calibration performed under the same experimental conditions. It is necessary to point out that the magnetic field in our study is reasonably homogeneous. The typical mean and standard deviation of B_0 inhomogeneity is within 5 and 10 Hz, respectively. We used a dual RF coil setup and the B_1 profile from the RF volume transmitter is of good homogeneity (Sun et al., 2007a). Indeed, MRAPT images appear homogeneous across the intact brain tissue.

It helps to briefly discuss the relationship between the commonly used perfusion and diffusion MRI and pH imaging. Although perfusion is sensitive to ischemia, the effect of hypoperfusion on tissue ischemic injury is highly variable, depending on the tissue susceptibility, duration of hypoperfusion and collateral flow. In addition, noninvasive ASL perfusion MRI is of relatively low signal to noise ratio (SNR) and may not fully resolve small regional perfusion difference. As such, it is difficult to rely on perfusion alone to further demarcate the hypoperfused ischemic tissue (Schellinger et al., 2010). Conversely, diffusion imaging is sensitive to severely injured ischemic tissue, and it cannot resolve penumbra from benign oligemia since none of these regions show diffusion abnormality. In comparison, tissue pH is tightly-regulated under normal physiological conditions, and pH shift is specific to glucose/oxygen metabolic disruption in acute stroke (Hossmann, 2006; Smith et al., 1990). It is helpful to compare pH MRI with results using complementary techniques such as radiographic imaging. Peek et al. used ^{14}C radiographic imaging and reported that pH in the regions of metabolic penumbra was 6.87 ± 0.05 while regions of severe acidosis with reduced glucose metabolism had a pH of 6.69 ± 0.11 (Peek et al., 1989). In comparison, our study documented pH from the perfusion/diffusion lesion mismatch was 6.84 ± 0.10 . In addition, pH from the pH/diffusion lesion mismatch area was 6.71 ± 0.12 . As diffusion lesion was poorly perfused with radiotracers, our results appeared in good agreement with those from radiographic imaging. Therefore, absolute pH map based on MRAPT MRI may provide a surrogate metabolic imaging biomarker to augment perfusion and diffusion MRI, help predict heterogeneous tissue response to recanalization, and ultimately, be translated and guide late recanalization in the clinical setting (Harston et al., 2015; Leslie-Mazwi et al., 2016; Rebello et al., 2017).

Our work built on the recent MRAPT approach, calibrated it for absolute pH mapping, and further determined tissue pH in benign oligemia, ischemic penumbra, and infarction regions.

Zhou et al. first demonstrated APT MRI in acute stroke animal model, providing the initial evidence that it is pH sensitive (Zhou et al., 2003). Since then, persistent progress has been achieved in CEST MRI quantification and optimization, yet in vivo tissue pH quantification has been challenging (Jones et al., 2018; Kim et al., 2015; Liu et al., 2013). Most work thus far used pH-weighted MRI and manual lesion segmentation has been used in experimental stroke research and acute stroke patients, limiting its adoption (Harston et al., 2015; Sun et al., 2007c; Tietze et al., 2014). Recently, Jin et al. proposed to combine guanidyl- and amide- CEST effects for improved pH calibration at 9.4 T (Jin et al., 2017). However, pH-dependent exchange properties of guanidyl and amide protons are very different, albeit pH sensitive, which may confound pH mapping (Heo et al., 2016). It has been noted that there are multiple saturation transfer effects that may complement each other for pH imaging (Desmond and Stanisiz, 2012; Heo et al., 2016; Jin et al., 2013; Zaiss et al., 2014; Zhang et al., 2016). We have recently decoupled contributions from amide, guanidyl, and NOE effects, and concluded that under a moderate RF irradiation, amide exchange dominates guanidyl and NOE contrast during the acute stroke (Wu et al., 2018). The development of pH-specific MRAPT MRI minimizes non-pH concomitant effects, permitting semi-automated segmentation of heterogeneous ischemic tissue (Guo et al., 2016). The MRAPT analysis only requires regression analysis without resorting to non-linear multi-parametric fitting and therefore is relatively straightforward to implement. Although CEST MRI measurement depends on the experimental conditions, in particular, the RF saturation field, we have chosen a B_1 field previously optimized for pH-weighted MRI at 4.7 T. Admittedly, the optimal experimental protocol for pH imaging depends on the experimental conditions and field strength (Sun et al., 2013). A systematic optimization and calibration experiments are needed before we translate non-invasive absolute pH mapping to the clinic.

Our study chose lactate over phosphorous MRS for pH calibration because proton lactate spectroscopy is of higher sensitivity and easier to implement. We chose a long echo time of 144 ms so that the lactate peak is unmistakably inverted to improve its specificity. Moreover, the use of lactate MRS for pH determination is supported by the observations that in permanent ischemia, the correlation between lactate concentration and intracellular pH determined from phosphorous MRS is very strong (Chang et al., 1990; Hohn-Berlage et al., 1989). This is consistent with our observation that intracellular pH sensitized by APT MRI is closely correlated with lactate pH MRS. Nevertheless, our study has a few limitations. Although our study assumed that diffusion lesion captures the most severely injured ischemic core tissue, it is important to recognize that DWI lesion contains graded change of metabolites and neuronal markers, and DWI lesion may not synonymous with infarction core (Geisler et al., 2006; Guadagno et al., 2006; Nicoli et al., 2003). A number of studies documented DWI reversibility following recanalization, even in some cases of large DWI lesions (Yamada et al., 2012; Yoo et al., 2010). Recent studies have documented that kurtosis lesion shows poor response to hyperacute reperfusion while kurtosis/diffusion lesion mismatch responds favorably to reperfusion, suggesting graded tissue damage within the routine diffusion lesion, which shall be further investigated (Cheung et al., 2012; Lu et al., 2018; Wang et al., 2017; Weber et al., 2015; Yin et al., 2018). In addition, although pH MRI values agreed well with those of Peek et al., ^{14}C autoradiographic imaging is technically challenging and not readily available. We could not calibrate pH MRI with radiographic

imaging in our present study. Moreover, T_{1w} MRI is needed for MRAPT analysis. Fortunately, T_{1w} mapping only takes a few minutes. The scan time can be shortened using techniques such as fingerprinting (Anderson et al., 2018; Doerr, 2013) and look-locker MRI (Henderson et al., 1999; Zhang et al., 1992). Note that the current study was performed on rats at hyperacute stroke stage, and confounding factor such as relaxation, MT, edema have to be considered in order to extend pH mapping to the subacute stroke setting. Furthermore, our current study only investigated rodents under the normoglycemic condition, and the inclusion of animals with hyperglycemic preconditioning will extend the dynamic range of pH change. This will not only improve the accuracy of pH calibration but also is highly relevant to acute stroke patients who often present with comorbidities such as diabetes.

Conclusion

Our study calibrated pH-sensitive MRAPT MRI toward absolute tissue pH mapping and delineated ischemic tissue based on its hemodynamic, metabolic and diffusion indices. We documented graded tissue pH from the benign oligemia (7.01 ± 0.04), ischemic penumbra (6.71 ± 0.12) and the infarction core (6.52 ± 0.19). Non-invasive tissue pH mapping provides a metabolic imaging biomarker for the identification of heterogeneous ischemic tissue injury.

Acknowledgments:

This study was supported in part by grants from NIH R01NS083654 (Sun).

REFERENCES

- Anderson CE, Wang CY, Gu Y, Darrah R, Griswold MA, Yu X, Flask CA, 2018 Regularly incremented phase encoding - MR fingerprinting (RIPE-MRF) for enhanced motion artifact suppression in preclinical cartesian MR fingerprinting. *Magnetic Resonance in Medicine* 79, 2176–2182. [PubMed: 28796368]
- Anderson RE, Tan WK, Martin HS, Meyer FB, 1999 Effects of glucose and PaO₂ modulation on cortical intracellular acidosis, NADH redox state, and infarction in the ischemic penumbra. *Stroke* 30, 160–170. [PubMed: 9880405]
- Astrup J, Siesjo BK, Symon L, 1981 Thresholds in cerebral ischemia - the ischemic penumbra. *Stroke* 12, 723–725. [PubMed: 6272455]
- Chang LH, Shirane R, Weinstein PR, James TL, 1990 Cerebral metabolite dynamics during temporary complete ischemia in rats monitored by time-shared ¹H and ³¹P NMR spectroscopy. *Magnetic Resonance in Medicine* 13, 6–13. [PubMed: 2319935]
- Cheung JS, Wang E, Lo EH, Sun PZ, 2012 Stratification of heterogeneous diffusion MRI ischemic lesion with kurtosis imaging: evaluation of mean diffusion and kurtosis MRI mismatch in an animal model of transient focal ischemia. *Stroke* 43, 2252–2254. [PubMed: 22773558]
- Desmond KL, Stanisz GJ, 2012 Understanding quantitative pulsed CEST in the presence of MT. *Magnetic Resonance in Medicine* 67, 979–990. [PubMed: 21858864]
- Doerr A, 2013 Imaging: Fingerprinting with MRI. *Nat Meth* 10, 380–381.
- Geisler BS, Brandhoff F, Fiehler J, Saager C, Speck O, Rother J, Zeumer H, Kucinski T, 2006 Blood-oxygen-level-dependent MRI allows metabolic description of tissue at risk in acute stroke patients. *Stroke* 37, 1778–1784. [PubMed: 16741186]
- Guadagno JV, Warburton EA, Jones PS, Day DJ, Aigbirhio FI, Fryer TD, Harding S, Price CJ, Green HA, Barret O, Gillard JH, Baron JC, 2006 How affected is oxygen metabolism in DWI lesions?: A combined acute stroke PET-MR study. *Neurology* 67, 824–829. [PubMed: 16966545]
- Guo Y, Zhou IY, Chan ST, Wang Y, Mandeville ET, Igarashi T, Lo EH, Ji X, Sun PZ, 2016 pH-sensitive MRI demarcates graded tissue acidification during acute stroke - pH specificity

enhancement with magnetization transfer and relaxation-normalized amide proton transfer (APT) MRI. *Neuroimage* 141, 242–249. [PubMed: 27444569]

- Harston GW, Tee YK, Blockley N, Okell TW, Thandeswaran S, Shaya G, Sheerin F, Cellnerini M, Payne S, Jezzard P, Chappell M, Kennedy J, 2015 Identifying the ischaemic penumbra using pH-weighted magnetic resonance imaging. *Brain* 138, 36–42. [PubMed: 25564491]
- Henderson E, McKinnon G, Lee TY, Rutt BK, 1999 A fast 3D look-locker method for volumetric T1 mapping. *Magnetic Resonance Imaging* 17, 1163–1171. [PubMed: 10499678]
- Heo HY, Zhang Y, Burton TM, Jiang S, Zhao Y, van Zijl PCM, Leigh R, Zhou J, 2017 Improving the detection sensitivity of pH-weighted amide proton transfer MRI in acute stroke patients using extrapolated semisolid magnetization transfer reference signals. *Magnetic Resonance in Medicine* 78, 871–880. [PubMed: 28639301]
- Heo HY, Zhang Y, Jiang S, Lee DH, Zhou J, 2016 Quantitative assessment of amide proton transfer (APT) and nuclear overhauser enhancement (NOE) imaging with extrapolated semisolid magnetization transfer reference (EMR) signals: II. Comparison of three EMR models and application to human brain glioma at 3 Tesla. *Magnetic Resonance in Medicine* 75, 1630–1639. [PubMed: 26033553]
- Hohn-Berlage M, Okada Y, Kloiber O, Hossmann KA, 1989 Imaging of brain tissue pH and metabolites. A new approach for the validation of volume-selective NMR spectroscopy. *NMR in Biomedicine* 2, 240–245. [PubMed: 2701807]
- Hossmann KA, 1994 Viability thresholds and the penumbra of focal ischemia. *Annals of Neurology* 36, 557–565. [PubMed: 7944288]
- Hossmann KA, 2006 Pathophysiology and therapy of experimental stroke. *Cellular and Molecular Neurobiology* 26, 1057–1083. [PubMed: 16710759]
- Jin T, Kim SG, 2014 Advantages of chemical exchange-sensitive spin-lock (CESL) over chemical exchange saturation transfer (CEST) for hydroxyl- and amine-water proton exchange studies. *NMR in Biomedicine* 27, 1313–1324. [PubMed: 25199631]
- Jin T, Wang P, Hitchens TK, Kim SG, 2017 Enhancing sensitivity of pH-weighted MRI with combination of amide and guanidyl CEST. *Neuroimage* 157, 341–350. [PubMed: 28602944]
- Jin T, Wang P, Zong X, Kim SG, 2013 MR imaging of the amide-proton transfer effect and the pH-insensitive nuclear overhauser effect at 9.4 T. *Magnetic Resonance in Medicine* 69, 760–770. [PubMed: 22577042]
- Jokivarsi KT, Grohn HI, Grohn OH, Kauppinen RA, 2007 Proton transfer ratio, lactate, and intracellular pH in acute cerebral ischemia. *Magnetic Resonance in Medicine* 57, 647–653. [PubMed: 17390356]
- Jones KM, Pollard AC, Pagel MD, 2018 Clinical applications of chemical exchange saturation transfer (CEST) MRI. *Journal of Magnetic Resonance Imaging* 47, 11–27. [PubMed: 28792646]
- Katsura K, Asplund B, Ekholm A, Siesjo BK, 1992 Extra- and Intracellular pH in the Brain During Ischaemia, Related to Tissue Lactate Content in Normo- and Hypercapnic rats. *European Journal of Neuroscience* 4, 166–176. [PubMed: 12106379]
- Kidwell CS, Alger JR, Saver JL, 2004 Evolving paradigms in neuroimaging of the ischemic penumbra. *Stroke* 35, 2662–2665. [PubMed: 15472112]
- Kim J, Wu Y, Guo Y, Zheng H, Sun PZ, 2015 A review of optimization and quantification techniques for chemical exchange saturation transfer MRI toward sensitive in vivo imaging. *Contrast Media & Molecular Imaging* 10, 163–178. [PubMed: 25641791]
- Leslie-Mazwi TM, Hirsch JA, Falcone GJ, Schaefer PW, Lev MH, Rabinov JD, Rost NS, Schwamm L, Gonzalez RG, 2016 Endovascular Stroke Treatment Outcomes After Patient Selection Based on Magnetic Resonance Imaging and Clinical Criteria. *JAMA Neurology* 73, 43–49. [PubMed: 26524074]
- Liu G, Song X, Chan KW, McMahon MT, 2013 Nuts and bolts of chemical exchange saturation transfer MRI. *NMR in Biomedicine* 26, 810–828. [PubMed: 23303716]
- Lu D, Jiang Y, Ji Y, Zhou IY, Mandeville E, Lo EH, Wang X, Sun PZ, 2018 JOURNAL CLUB: Evaluation of Diffusion Kurtosis Imaging of Stroke Lesion With Hemodynamic and Metabolic MRI in a Rodent Model of Acute Stroke. *AJR. American Journal of Roentgenology* 210, 720–727. [PubMed: 29470156]

- McVicar N, Li AX, Goncalves DF, Bellyou M, Meakin SO, Prado MA, Bartha R, 2014 Quantitative tissue pH measurement during cerebral ischemia using amine and amide concentration-independent detection (AACID) with MRI. *Journal of Cerebral Blood Flow and Metabolism* 34, 690–698. [PubMed: 24496171]
- Mehrabian H, Myrehaug S, Soliman H, Sahgal A, Stanisz GJ, 2018 Evaluation of Glioblastoma Response to Therapy With Chemical Exchange Saturation Transfer. *International Journal of Radiation Oncology, Biology, & Physics* 101, 713–723.
- Mori S, Vanzijl PCM, 1995 Diffusion Weighting by the Trace of the Diffusion Tensor within a Single Scan. *Magnetic Resonance in Medicine* 33, 41–52. [PubMed: 7891534]
- Naruse S, Takada S, Koizuka I, Watari H, 1983 In vivo 31P NMR studies on experimental cerebral infarction. *Japanese Journal of Physiology* 33, 19–28. [PubMed: 6855029]
- Nicoli F, Lefur Y, Denis B, Ranjeva JP, Confort-Gouny S, Cozzzone PJ, 2003 Metabolic counterpart of decreased apparent diffusion coefficient during hyperacute ischemic stroke: a brain proton magnetic resonance spectroscopic imaging study. *Stroke* 34, e82–87. [PubMed: 12817104]
- Peek KE, Lockwood AH, Izumiyama M, Yap EW, Labove J, 1989 Glucose metabolism and acidosis in the metabolic penumbra of rat brain. *Metabolic Brain Disease* 4, 261–272. [PubMed: 2601642]
- Rebello LC, Bouslama M, Haussen DC, Dehkharghani S, Grossberg JA, Belagaje S, Frankel MR, Nogueira RG, 2017 Endovascular Treatment for Patients With Acute Stroke Who Have a Large Ischemic Core and Large Mismatch Imaging Profile. *JAMA Neurology* 74, 34–40. [PubMed: 27820620]
- Regli L, Anderson RE, Meyer FB, 1995 Effects of intermittent reperfusion on brain pHi, rCBF, and NADH during rabbit focal cerebral ischemia. *Stroke* 26, 1444–1451; [PubMed: 7631351]
- Schellinger PD, Bryan RN, Caplan LR, Detre JA, Edelman RR, Jaigobin C, Kidwell CS, Mohr JP, Sloan M, Sorensen AG, Warach S, Therapeutics, Technology Assessment Subcommittee of the American Academy of Neurology, 2010 Evidence-based guideline: The role of diffusion and perfusion MRI for the diagnosis of acute ischemic stroke: report of the Therapeutics and Technology Assessment Subcommittee of the American Academy of Neurology. *Neurology* 75, 177–185. [PubMed: 20625171]
- Siesjo BK, 1992 Pathophysiology and treatment of focal cerebral ischemia: Part I: Pathophysiology. *Journal of Neurosurgery* 77, 169–184. [PubMed: 1625004]
- Smith CD, Thomas GS, Kryscio RJ, Markesbery WR, 1990 31P spectroscopy in experimental embolic stroke: correlation with infarct size. *NMR in Biomedicine* 3, 259–264. [PubMed: 2092741]
- Snoussi K, Gillen JS, Horska A, Puts NA, Pradhan S, Edden RA, Barker PB, 2015 Comparison of brain gray and white matter macromolecule resonances at 3 and 7 Tesla. *Magnetic Resonance in Medicine* 74, 607–613. [PubMed: 25252131]
- Sun PZ, Cheung JS, Wang E, Benner T, Sorensen AG, 2011a Fast multislice pH-weighted chemical exchange saturation transfer (CEST) MRI with Unevenly segmented RF irradiation. *Magnetic Resonance in Medicine* 65, 588–594. [PubMed: 20872859]
- Sun PZ, Cheung JS, Wang E, Lo EH, 2011b Association between pH-weighted endogenous amide proton chemical exchange saturation transfer MRI and tissue lactic acidosis during acute ischemic stroke. *Journal of Cerebral Blood Flow and Metabolism* 31, 1743–1750. [PubMed: 21386856]
- Sun PZ, Farrar CT, Sorensen AG, 2007a Correction for artifacts induced by B(0) and B(1) field inhomogeneities in pH-sensitive chemical exchange saturation transfer (CEST) imaging. *Magnetic Resonance in Medicine* 58, 1207–1215. [PubMed: 17969015]
- Sun PZ, Lu J, Wu Y, Xiao G, Wu R, 2013 Evaluation of the dependence of CEST-EPI measurement on repetition time, RF irradiation duty cycle and imaging flip angle for enhanced pH sensitivity. *Physics in Medicine and Biology* 58, N229–240. [PubMed: 23939228]
- Sun PZ, Wang E, Cheung JS, 2012 Imaging acute ischemic tissue acidosis with pH-sensitive endogenous amide proton transfer (APT) MRI--correction of tissue relaxation and concomitant RF irradiation effects toward mapping quantitative cerebral tissue pH. *Neuroimage* 60, 1–6. [PubMed: 22178815]
- Sun PZ, Zhou J, Huang J, van Zijl P, 2007b Simplified quantitative description of amide proton transfer (APT) imaging during acute ischemia. *Magnetic Resonance in Medicine* 57, 405–410. [PubMed: 17260362]

- Sun PZ, Zhou J, Sun W, Huang J, van Zijl PC, 2007c Detection of the ischemic penumbra using pH-weighted MRI. *Journal of Cerebral Blood Flow and Metabolism* 27, 1129–1136. [PubMed: 17133226]
- Tietze A, Blicher J, Mikkelsen IK, Ostergaard L, Strother MK, Smith SA, Donahue MJ, 2014 Assessment of ischemic penumbra in patients with hyperacute stroke using amide proton transfer (APT) chemical exchange saturation transfer (CEST) MRI. *NMR in Biomedicine* 27, 163–174. [PubMed: 24288260]
- Tomlinson FH, Anderson RE, Meyer FB, 1993 Brain pH, cerebral blood flow, and NADH fluorescence during severe incomplete global ischemia in rabbits. *Stroke* 24, 435–443. [PubMed: 8446980]
- Utting JF, Thomas DL, Gadian DG, Helliard RW, Lythgoe MF, Ordidge RJ, 2005 Understanding and optimizing the amplitude modulated control for multiple-slice continuous arterial spin labeling. *Magnetic Resonance in Medicine* 54, 594–604. [PubMed: 16086330]
- Wang E, Wu Y, Cheung JS, Zhou IY, Igarashi T, Zhang X, Sun PZ, 2017 pH imaging reveals worsened tissue acidification in diffusion kurtosis lesion than the kurtosis/diffusion lesion mismatch in an animal model of acute stroke. *Journal of Cerebral Blood Flow and Metabolism* 37, 3325–3333. [PubMed: 28752790]
- Warach S, 2003 Measurement of the ischemic penumbra with MRI: it's about time. *Stroke* 34, 2533–2534. [PubMed: 12970511]
- Ward KM, Aletras AH, Balaban RS, 2000 A new class of contrast agents for MRI based on proton chemical exchange dependent saturation transfer (CEST). *Journal of Magnetic Resonance* 143, 79–87. [PubMed: 10698648]
- Weber RA, Hui ES, Jensen JH, Nie X, Falangola MF, Helpert JA, Adkins DL, 2015 Diffusional kurtosis and diffusion tensor imaging reveal different time-sensitive stroke-induced microstructural changes. *Stroke* 46, 545–550. [PubMed: 25563646]
- Wu R, Liu CM, Liu PK, Sun PZ, 2012 Improved measurement of labile proton concentration-weighted chemical exchange rate (k(ws)) with experimental factor-compensated and T(1) -normalized quantitative chemical exchange saturation transfer (CEST) MRI. *Contrast Media & Molecular Imaging* 7, 384–389. [PubMed: 22649044]
- Wu Y, Zhou IY, Lu D, Manderville E, Lo EH, Zheng H, Sun PZ, 2018 pH-sensitive amide proton transfer effect dominates the magnetization transfer asymmetry contrast during acute ischemia-quantification of multipool contribution to in vivo CEST MRI. *Magnetic Resonance in Medicine* 79, 1602–1608. [PubMed: 28733991]
- Xu X, Yadav NN, Zeng H, Jones CK, Zhou J, van Zijl PC, Xu J, 2016 Magnetization transfer contrast-suppressed imaging of amide proton transfer and relayed nuclear overhauser enhancement chemical exchange saturation transfer effects in the human brain at 7T. *Magnetic Resonance in Medicine* 75, 88–96. [PubMed: 26445350]
- Yamada R, Yoneda Y, Kageyama Y, Ichikawa K, 2012 Reversal of large ischemic injury on hyperacute diffusion MRI. *Case Rep Neurol* 4, 177–180. [PubMed: 23185171]
- Yin J, Sun H, Wang Z, Ni H, Shen W, Sun PZ, 2018 Diffusion Kurtosis Imaging of Acute Infarction: Comparison with Routine Diffusion and Follow-up MR Imaging. *Radiology* 287, 651–657. [PubMed: 29558293]
- Yoo AJ, Hakimelahi R, Rost NS, Schaefer PW, Hirsch JA, Gonzalez RG, Rabinov JD, 2010 Diffusion weighted imaging reversibility in the brainstem following successful recanalization of acute basilar artery occlusion. *J Neurointerv Surg* 2, 195–197. [PubMed: 21990621]
- Zaiss M, Xu J, Goerke S, Khan IS, Singer RJ, Gore JC, Gochberg DF, Bachert P, 2014 Inverse Z-spectrum analysis for spillover-, MT-, and T1 -corrected steady-state pulsed CEST-MRI--application to pH-weighted MRI of acute stroke. *NMR in Biomedicine* 27, 240–252. [PubMed: 24395553]
- Zhang XY, Wang F, Afzal A, Xu J, Gore JC, Gochberg DF, Zu Z, 2016 A new NOE-mediated MT signal at around –1.6ppm for detecting ischemic stroke in rat brain. *Magnetic Resonance Imaging* 34, 1100–1106. [PubMed: 27211260]

- Zhang YT, Yeung HN, Carson PL, Ellis JH, 1992 Experimental analysis of T1 imaging with a single-scan, multiple-point, inversion-recovery technique. *Magnetic Resonance in Medicine* 25, 337–343. [PubMed: 1614317]
- Zhao X, Wen Z, Huang F, Lu S, Wang X, Hu S, Zu D, Zhou J, 2011 Saturation power dependence of amide proton transfer image contrasts in human brain tumors and strokes at 3 T. *Magnetic Resonance in Medicine* 66, 10331041.
- Zhou IY, Lu D, Ji Y, Wu L, Wang E, Cheung JS, Zhang XA, Sun PZ, 2019 Determination of multipool contributions to endogenous amide proton transfer effects in global ischemia with high spectral resolution in vivo chemical exchange saturation transfer MRI. *Magnetic Resonance in Medicine* 81, 645–652. [PubMed: 30058148]
- Zhou J, Payen JF, Wilson DA, Traystman RJ, van Zijl PC, 2003 Using the amide proton signals of intracellular proteins and peptides to detect pH effects in MRI. *Nature Medicine* 9, 1085–1090.
- Zhou J, van Zijl PC, 2011 Defining an Acidosis-Based Ischemic Penumbra from pH-Weighted MRI. *Transl Stroke Res* 3, 76–83. [PubMed: 22408691]
- Zhou J, Wilson DA, Sun PZ, Klaus JA, Van Zijl PC, 2004 Quantitative description of proton exchange processes between water and endogenous and exogenous agents for WEX, CEST, and APT experiments. *Magnetic Resonance in Medicine* 51, 945–952. [PubMed: 15122676]
- Zhu XH, Qiao H, Du F, Xiong Q, Liu X, Zhang X, Ugurbil K, Chen W, 2012 Quantitative imaging of energy expenditure in human brain. *Neuroimage* 60, 2107–2117. [PubMed: 22487547]
- Zu Z, Afzal A, Li H, Xie J, Gore JC, 2018 Spin-lock imaging of early tissue pH changes in ischemic rat brain. *NMR in Biomedicine* 31, e3893. [PubMed: 29424463]

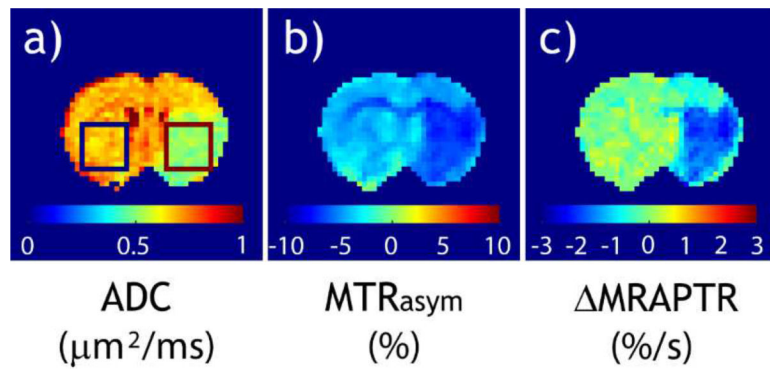


Figure 1,
MRI images of a representative acute stroke rat. a) ADC image with the overlaid ipsilateral ischemic ROI (red) and the contralateral normal ROI (blue). b) pH-weighted MTR_{asym} image. c) pH-specific ΔMRAPTR image. ADC=apparent diffusion coefficient, MTR_{asym} =magnetization transfer ratio asymmetry, ΔMRAPTR = magnetization transfer, and relaxation corrected amide proton transfer ratio.

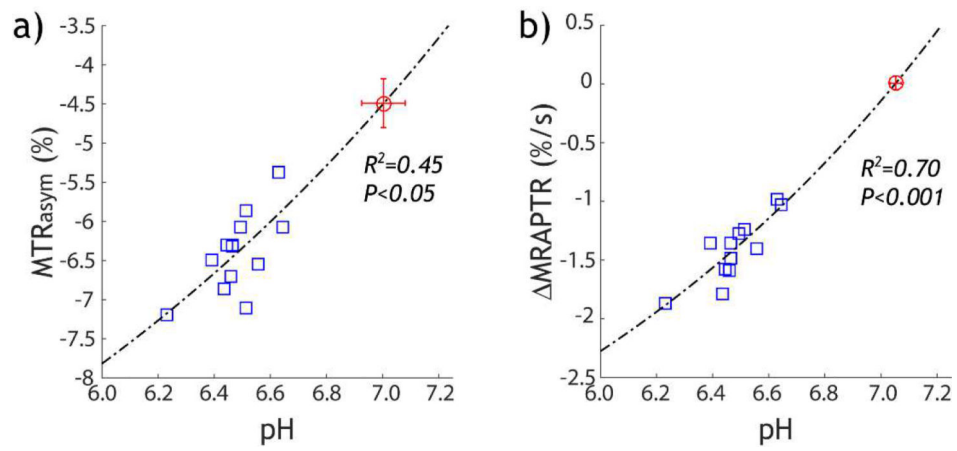


Figure 2,
Calibration of pH-sensitive APT MRI indices (MTR_{asy} and Δ MRAPTR) toward absolute tissue pH from stroke rats with both MRI and MRS scans (N=15). a) MTR_{asy} vs. pH, and b) Δ MRAPTR vs. pH. MTR_{asy} =magnetization transfer ratio asymmetry, Δ MRAPTR=magnetization transfer, and relaxation corrected amide proton transfer ratio.

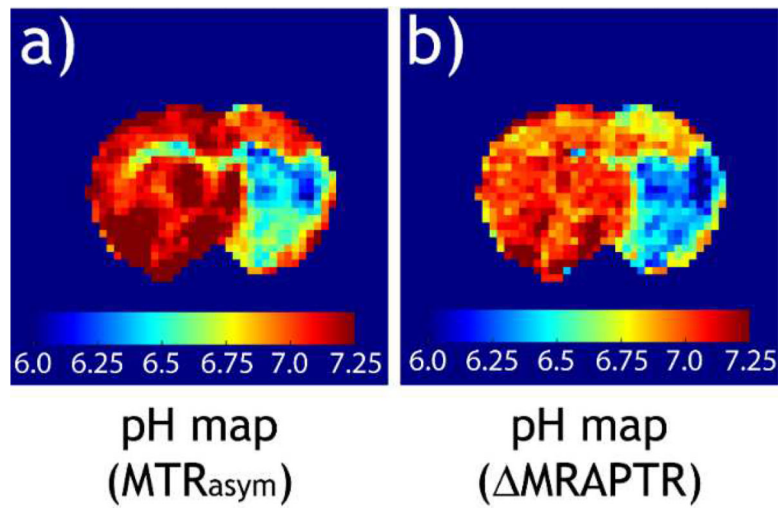


Figure 3,
pH images from a representative acute stroke rat. a) pH map from MTR_{asyM} image. b) pH map from MRAPTR image. MTR_{asyM}=magnetization transfer ratio asymmetry, MRAPTR= magnetization transfer, and relaxation corrected amide proton transfer ratio.

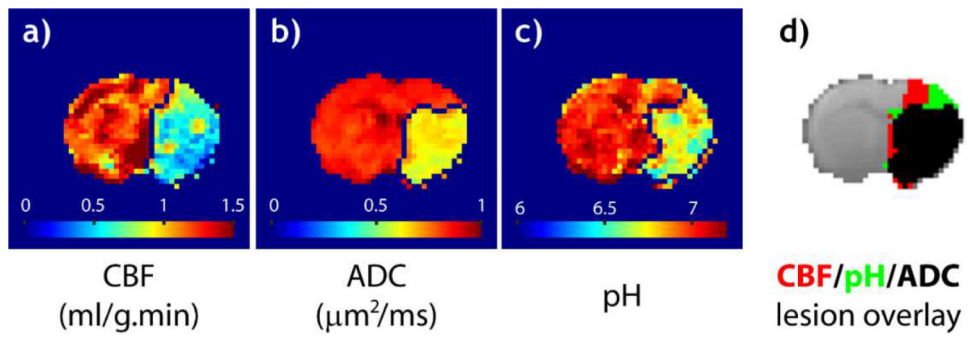


Figure 4,
Multi-parametric images of a representative acute stroke rat. a) perfusion image. b) diffusion image. c) pH map determined from MRAPTR image. d) paradigm of perfusion/pH/diffusion lesion mismatch. CBF=cerebral blood flow, ADC=apparent diffusion coefficient.

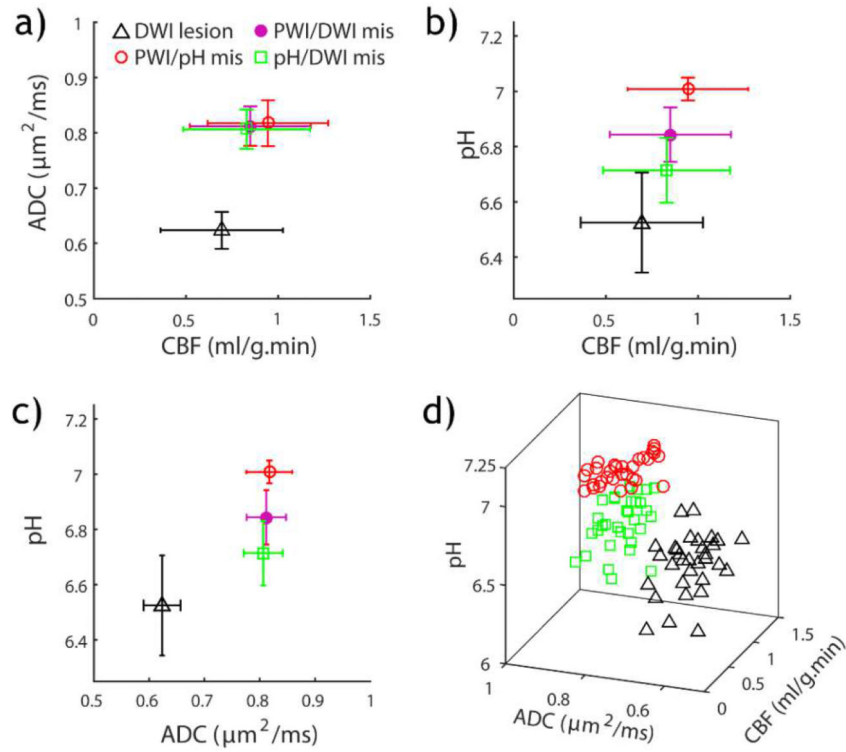


Figure 5,
 Comparison of perfusion, pH and diffusion indices from diffusion lesion, pH/diffusion lesion mismatch, perfusion/pH lesion mismatch and perfusion/diffusion mismatch from all animals (N=35). a) ADC vs. CBF. b) pH vs. CBF. c) pH vs. ADC. d) Three-dimensional stratification of CBF, ADC and pH indices from diffusion lesion, pH/diffusion lesion mismatch, and perfusion/pH lesion mismatch. CBF=cerebral blood flow, ADC=apparent diffusion coefficient.

Table 1.

Calibration of ROI-based pH-sensitive MRI (MTR_{asym} and $MRAPTR$) against pH determined from lactate MRS (N=15), using a base-catalyzed exchange rate relationship. Both $MRAPTR$ and MTR_{asym} significantly correlated with pH, with $MRAPTR$ showing a noticeably higher correlation with pH than MTR_{asym} .

	Contralateral Normal ROI	Ipsilateral Ischemic ROI	
	pH (MRI)	pH (MRI)	R ²
MTR_{asym} (%)	7.00 ± 0.08	6.48 ± 0.15	0.45 *
$MRAPTR$ (%/s)	7.05 ± 0.02	6.48 ± 0.13	0.70 **

*
(P<0.05)

**
(P<0.001).

Table 2.

Multi-parametric perfusion, pH and diffusion states of graded ischemic tissue injury. pH shows little acidosis in the PWI/pH lesion mismatch (benign oligemia) from the intact tissue. It also captured worsened acidosis from pH/diffusion lesion mismatch (metabolic penumbra) to diffusion lesion (core).

	Contralateral Normal tissue	ADC Lesion (Core)	PWI/DWI lesion Mismatch (Conventional Penumbra)	PWI/pH lesion Mismatch (Benign Oligemia)	pH/ADC lesion mismatch (Metabolic Penumbra)
CBF (ml/g.min)	1.59±0.44	0.69±0.33	0.85±0.33	0.95±0.33	0.83±0.35
ADC ($\mu\text{m}^2/\text{ms}$)	0.83±0.03	0.62±0.03	0.81±0.04	0.82±0.04	0.81±0.04
pH	7.04±0.01	6.52±0.19	6.84±0.10	7.01±0.04	6.71±0.12

Author Manuscript

Author Manuscript

Author Manuscript

Author Manuscript